ON THE INTERPRETATION OF L- AND P-BAND POLSAR SIGNATURES OF POLYTHERMAL GLACIERS

G. Parrella[(1),(2)], I. Hajnsek[(1),(2)] & K. Papathanassiou[(1)]

[(1)] German Aerospace Center - Microwaves and Radar Institute, Oberpfaffenhofen, 82234 Wessling, Germany
[(2)] ETH Zurich - Institute of Environmental Engineering, Wolfgang-Pauli-Str. 15, CH-8093 Zurich, Switzerland
giuseppe.parrella@dlr.de, irena.hajnsek@dlr.de, kostas.papathanassiou@dlr.de

ABSTRACT

Long-wavelength SAR backscattering from glacier ice is of high relevance for glaciological applications since it contains information about both surface and subsurface structure of the ice. For this reason, SAR sensors can be used to discriminate and delineate the different glacier facies and to extract information on the ice density, which today can only be estimated on point basis.
In this paper, the authors focus on the modeling of polarimetric SAR (Pol-SAR) signatures of the percolation zone of the Austfonna ice cap, in the Svalbard archipelago, Norway. Incidence angle and frequency dependencies are deeply investigated and included in the model. A first assessment of the proposed model is finally performed by comparison with L- and P-band airborne Pol-SAR data collected by DLR's E-SAR system over the selected test site in 2007, during the ICESAR campaign.

Key Words: Polarimetric SAR, glacier ice, volume scattering, co-polarization phase difference, percolation zone.

1. INTRODUCTION

The use of airborne and satellite remote sensing techniques for glaciological applications led to significant improvements in scale as well as temporal and spatial resolution of cryospheric observations. Nevertheless, large uncertainties remain in estimating reliably glacier mass balance, accumulation rates and subsurface/volume structures. Due to their capability to penetrate several meters into the ice, SAR sensors represent the most promising tool to fill this gap. A straightforward and exhaustive link between Pol-SAR observables and physics of the scattering scenario can be provided by electromagnetic (e.m.) models specifically developed for a certain environment or application. Together with the very high resolution of current SAR sensors, they could be used to increase the accuracy of glaciers facies delineation and classification. Moreover, using multi-temporal SAR acquisitions, e.m. models have the potential to provide a better understanding of glaciers dynamics, monitoring the extent of the various facies and mass balance fluctuations occurring in the polar regions as a result of climatic changes. Nevertheless, the backscatter modeling and interpretation for this kind of scenario is still in an early stage, constrained by the complexity of the involved scattering mechanisms.
A first e.m. model was proposed in [1] to explain multi-frequency polarimetric signatures from the percolation zone of Greenland. The author attributes most of the scattering to ice pipes and lenses located in the shallow snow layer of the ice sheet and modeled as icy cylinders embedded in a transparent background. Despite this model was able to interpret many of the observed signatures, some others, e.g. the polarization phase differences, could not be exhaustively explained. In recent years a great attention has been given to model-based decomposition approaches. For glacier ice scenarios, a first model was proposed in [2] as adaptation of conventional 3-component polarimetric decomposition models. The total scattering was modeled as sum of different contributions: one attributed to a shallow snow-ice interface, a second contribution due to the underlying ice volume (of possibly oriented dipoles), and a third component associated to the eventual presence of oriented sastrugi on the glacier surface. Nevertheless, also this approach showed its main limitation in predicting polarization phase differences observed in the SAR data.
In this paper the authors attempt to provide a detailed interpretation of the polarimetric signatures observed in the selected dataset. For this, a dedicated model is presented for the case of the percolation zone.

2. PARTICLE MODEL FOR PERCOLATION ZONE

The approach proposed in this work addresses the interpretation of PolSAR signatures of a sub-polar ice-cap through the development of a volume scattering model. As suggested in [3] and [4], in the case of the percolation zone, most of the backscattering is attributable to the massive presence of solid ice clusters (pipes and lenses) in the upper meters of firn. In comparison, any other possible backscattering mechanism generated for instance at the air/snow interface on the glacier surface, or in the deeper volume of glacier ice is considered negligible. In fact, ice pipes and lenses typically extend for few tens of cm (comparable to the L-band wavelength) with a thickness of some cm. They are formed by internal refreezing of melt water occurring during summer at the glacier surface. The water percolates downward through small vertical channels and forms horizontal ice lenses and vertical pipes when the channels themselves get refrozen. Consequently, in this study, ice lenses are modeled as a cloud of mainly horizontally oriented oblate spheroids, whereas pipes are seen as a cloud of prolate spheroids, mainly oriented along the vertical direction. The scattering from a single and a cloud of spheroids is modeled as proposed in [5] by means of the covariance matrix. Assuming the scattering contributions from lenses and pipes are uncorrelated, the total covariance matrix can be expressed as sum of the matrices of the two scattering mechanisms:

$$[C]_{total} = f_{lenses}[C]_{lenses} + f_{pipes}[C]_{pipes} \qquad (1).$$

In particular, the term $[C]_{lenses}$ refers to a cloud of oblates ($x_1 < x_2 = x_3$) with shape factor $A_p = x_2 / x_1 = 0.01$ (see Fig.1), and uniform orientation angle distributions defined by the following angular pdfs:

$$p_1(\tau) = \frac{\cos\tau}{\sin\tau_2 - \sin\tau_1} \quad \text{for} \quad \tau_1 < \tau < \tau_2 \quad , 0 \text{ elsewhere} \qquad (2a)$$

$$p_2(\varphi) = \frac{1}{\varphi_2 - \varphi_1} \quad \text{for} \quad \varphi_1 < \varphi < \varphi_2 \quad , 0 \text{ elsewhere} \qquad (2b)$$

The tilt angle τ is allowed to vary from $-\pi/4$ to $-\pi/4$ (limited rotation about the horizontal plane x-y), whereas the canting angle φ is completely random ($\varphi_1 = 0$, $\varphi_2 = 2\pi$) allowing the horizontal particles to have all the possible orientation in the x-y plane (see Fig. 1). The term $[C]_{pipes}$ accounts for the cloud of prolates ($x_1 > x_2 = x_3$) with $A_p = 10$, tilt angle ranging from $\pi/4$ to $3/4\pi$ and mean value of $\pi/2$ (i.e. parallel to z-axis), and completely random canting angle. Finally, f_{lenses} and f_{pipes} are intensity factors of the two covariance matrices. Fig.1 shows the reference frame defined for a single spheroidal particle in the 3-dimensional space as well as the radar frame, illustrated by the propagation vector $\underline{k}$ and the wave component in the horizontal ($\underline{h}$) and vertical ($\underline{v}$) polarization.

Since the ice pipes and lenses are embedded in a background of firn, the modeling has to account also for the properties of the medium. In [6] the author investigated the structure of polar firn for remote sensing applications and concluded that it is clearly an anisotropic medium, very porous and made of slightly elongated ice grains (axial ratio ranging from 1.2 to 1.4), with preferred vertical orientation.

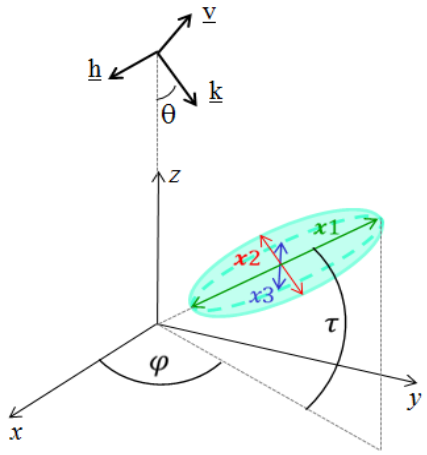

Figure 1: Orientation of a single spheroids in its local reference frame (x,y,z) and link to the radar reference frame (h,k,v).

In that study, the authors also suggest to model firn as a cloud of vertically oriented prolate spheroids. Based on these results and on the fact that firn (ice) grains are much smaller (<1mm) than the other scatterers (pipes and lenses) present in the investigated case, we believe that the volume scattering due to the grains is negligible whereas their anisotropy must be taken into account. In fact, an oriented volume of granular particles can be macroscopically considered as an anisotropic dielectric medium leading to different propagation velocities, phases and losses (if the permittivity is complex) along the different polarizations of an e.m. wave propagating through the medium itself [7]. This effect is modeled using the formulation proposed in [8] for the effective permittivity of a dielectric mixture of vertical prolates (ice grains) in a background of air. According to this formulation, the effective permittivity of firn along the different directions (x,y,z) can be written as:

$$\varepsilon_{eff,xyz} = \varepsilon_{air} + \mu_i \cdot \varepsilon_{air} \frac{\varepsilon_{ice} - \varepsilon_{air}}{\varepsilon_{air} + (1-\mu_i) N_{xyx} (\varepsilon_{ice} - \varepsilon_{air})} \qquad (3)$$

where μ_i is the particle volume fraction, ε_{air} and ε_{ice} the relative permittivity of the air background and ice grains, respectively, and N_{xyz} is depolarization factor of a single spheroidal grain along the directions x, y and z. For this study, a particle volume fraction μ_i = 60% is derived by

fixing a firn density ρ_{firn} = 0.55 kg/m^3. N_{xyz} are calculated for vertical prolates with axial ratio (i.e. shape factor) A_p = 1.3. Finally, values of ε_{air} = 1.0 and ε_{ice} = 3.15-j0.0008 are used for the relative permittivities of air and ice at L- and P-band [9], respectively. The model is completed with the inclusion of transmission effects occurring at the air/firn interface, at the glacier surface. For this, transmittivities for *H* and *V* polarization are approximated by the Fresnel formulation [10] and applied on the modeled covariance matrices $[C]_{lenses}$ and $[C]_{pipes}$. Including this effects, the complete model for the covariance matrix can be written as:

$$[C]_{total} = f_{lenses}[C]_{lenses} \circ [P] \circ [T] + f_{pipes}[C]_{pipes} \circ [P] \circ [T] \quad (4)$$

where [*T*] and [*P*] are 3x3 matrices accounting for transmission and differential propagation effects, respectively, whereas the operator ◦ represents the element-wise product.

3. TEST SITE AND AVAILABLE DATASET

The site selected for this study is located on the Austfonna ice-cap (79-80°N, 20-27°E), on the Nordaustlandet island of the Svalbard archipelago. Austfonna is a polythermal ice-cap with a dome-shaped topography, a maximum ice thickness of about 580m [11]. In particular, in this work we focus on the summit of the cap, classified as percolation zone, where L-band and P-band fully polarimetric SAR data were collected by the DLR's E-SAR airborne system during the ICESAR campaign, in March and April 2007. Repeat-pass acquisitions were performed with north and south flight directions. Fig. 2 shows a *Pauli*-RGB representation of one of the polarimetric scenes acquired in March for a first insight on the elementary scattering mechanisms. At L-band, the scene looks very homogeneous while at P-band several features become visible, probably due to buried structures revealed by the higher penetration capability of low frequencies.

4. EXPERIMENTAL RESULTS

To assess the qualitative performance of the developed scattering model, several polarimetric signatures have been simulated and compared to their counterparts observed in the experimental data. Among these, the authors focus the analysis on co-polarization ratio and phase difference (HH-VV), entropy (*H*) and mean alpha angle (α). Furthermore, *in-situ* investigations conducted on Austfonna in the same period as the SAR data collection, and published in [11], are used to support this study.

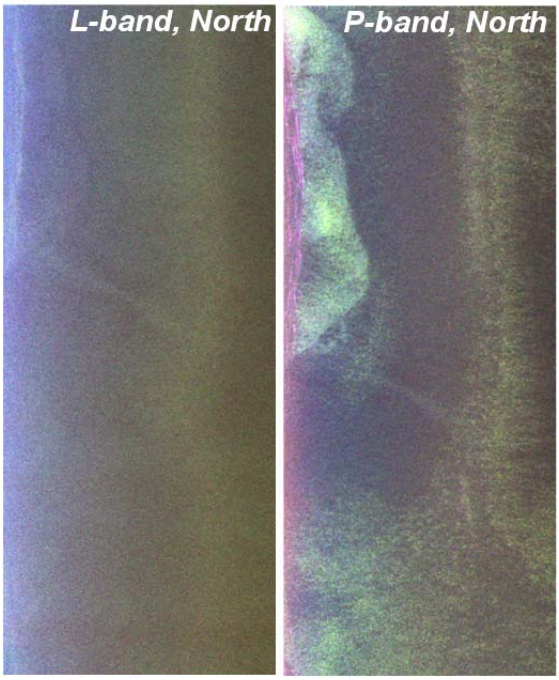

Figure 2: RGB *Pauli* images (R: 1/2<|S_{HH}-S_{VV}|>, G: 2<|S_{XX}|>, B: 1/2<|S_{HH}+S_{VV}|>) at L- and P-band for the North-heading on the "summit" test site; Left edge = near range.

From the modeled covariance matrix, a range profile of the selected signatures is generated by varying the incidence angle between 25° and 50°, in order to cover the same range of values used for the SAR acquisitions. The comparison is then performed by extracting range profiles of the signatures observed in the data by averaging along the entire azimuth dimension of the SAR scene (Fig. 3, 4). Range profiles of one of the north (red lines) and south (blue) acquisitions are shown together with the modeled profile when differential propagation effects are included (green) or neglected (purple). In particular, for the first case a firn layer of about 5m thickness is assumed, as suggested by in situ-measurements in [11]. For each data profile, standard deviations along azimuth direction are included for certain range positions. Fig. 3 shows the model-to-data comparison for the L-band case. The fact that north and south data profiles agree very well for all the signatures testifies that the investigated scenario is very homogeneous (it does not change with flight direction) and the observed linear trends can be attributed to the incidence angle dependency. In this case, the model matches quite well the signatures extracted from the data. The possibility to model the shape of the scatterers allows to explain the co-polarization ratio values and trend with the incidence angle. By comparing the green

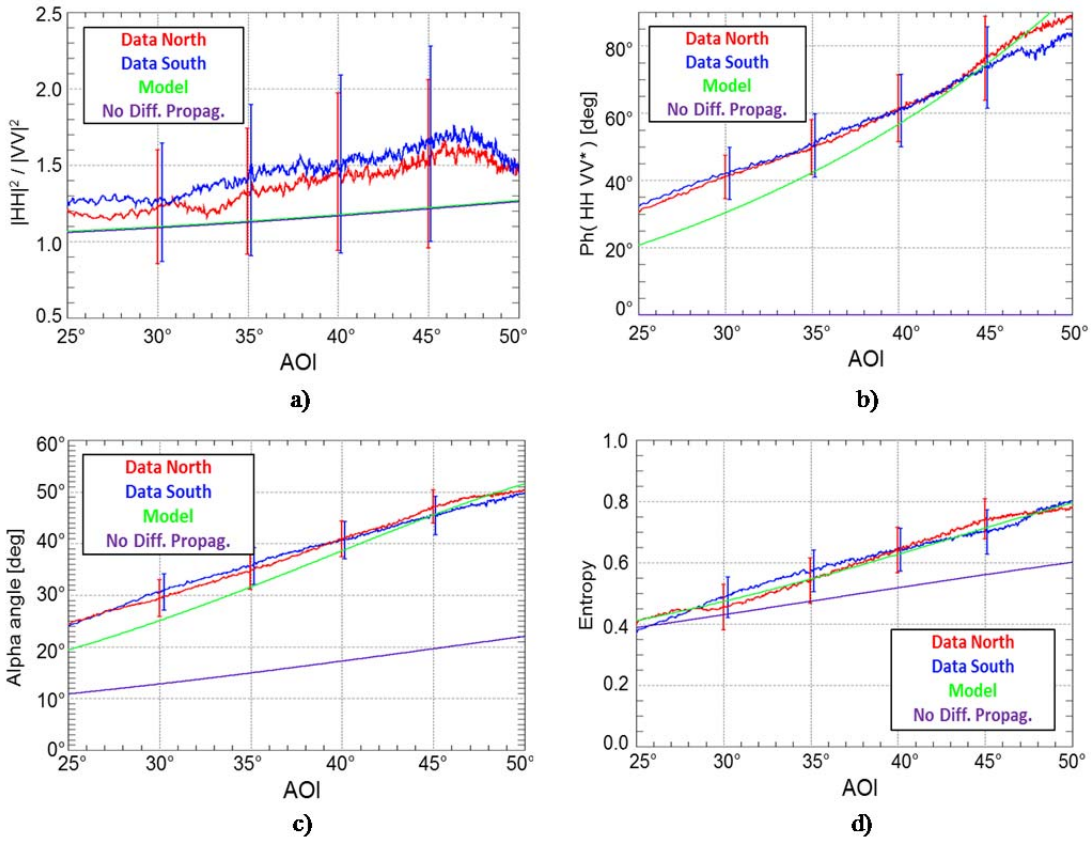

Figure 3: Model-to-data comparison of the selected polarimetric signatures at L-band: co-polarization ratio (a), co-polarization phase difference (b), mean alpha angle (c) and entropy (d). Red and blue lines refer to observed range profiles from the north and south heading, respectively; green lines depict modeled signatures when differential propagation effects are included whereas purple refer to the case that does not account for this phenomenon.

profiles to the purple ones, the impact of differential propagation due to the the firn anisotropy can be easily evaluated. In particular, the upper right graph in Fig. 3 clearly indicates that this phenomenon can explain the co-polarization phase difference and its trend along range observed in the data. Differential propagation also has a significant impact on H and α since it generally introduces a higher degree of diversity among the polarimetric channels.

For the case of P-band (Fig. 4), the polarimetric analysis of the data shows a different scenario compared to L-band. Modeled H and α values are still in good agreement with the data, if the deviation for the very near range (<30˚) is omitted. For the co-polarization phase, despite the observed range trend and the dynamics (around 50˚) are very similar to the L-band case, the anomalous negative values in the near range cannot be predicted by the model. Finally, the co-polarization ratio shows non-linear range trends, with significant disagreement between North and South heading. This could be explained by the presence of local buried icy structures, also visible in the *Pauli* image, and not included in the proposed model.

5. CONCLUSIONS

In this paper the authors presented a volume scattering model for the interpretation of polarimetric signatures observed in experimental L- and P-band airborne SAR data from the percolation zone of a polythermal ice-cap. As widely suggested in literature, most of the backscattering is assumed to be generated from ice clusters buried in the shallow firn layer (few meters) as result of refrozen meltwater. A negligible contribution is expected from the air/snow interface at the glacier surface and the volume of glacier ice underlying the firn layer, since it is very homogeneous (it shows only small density changes (layering) along depth) [11]. A set of polarimetric signatures has been selected to perform a first assessment of the model.

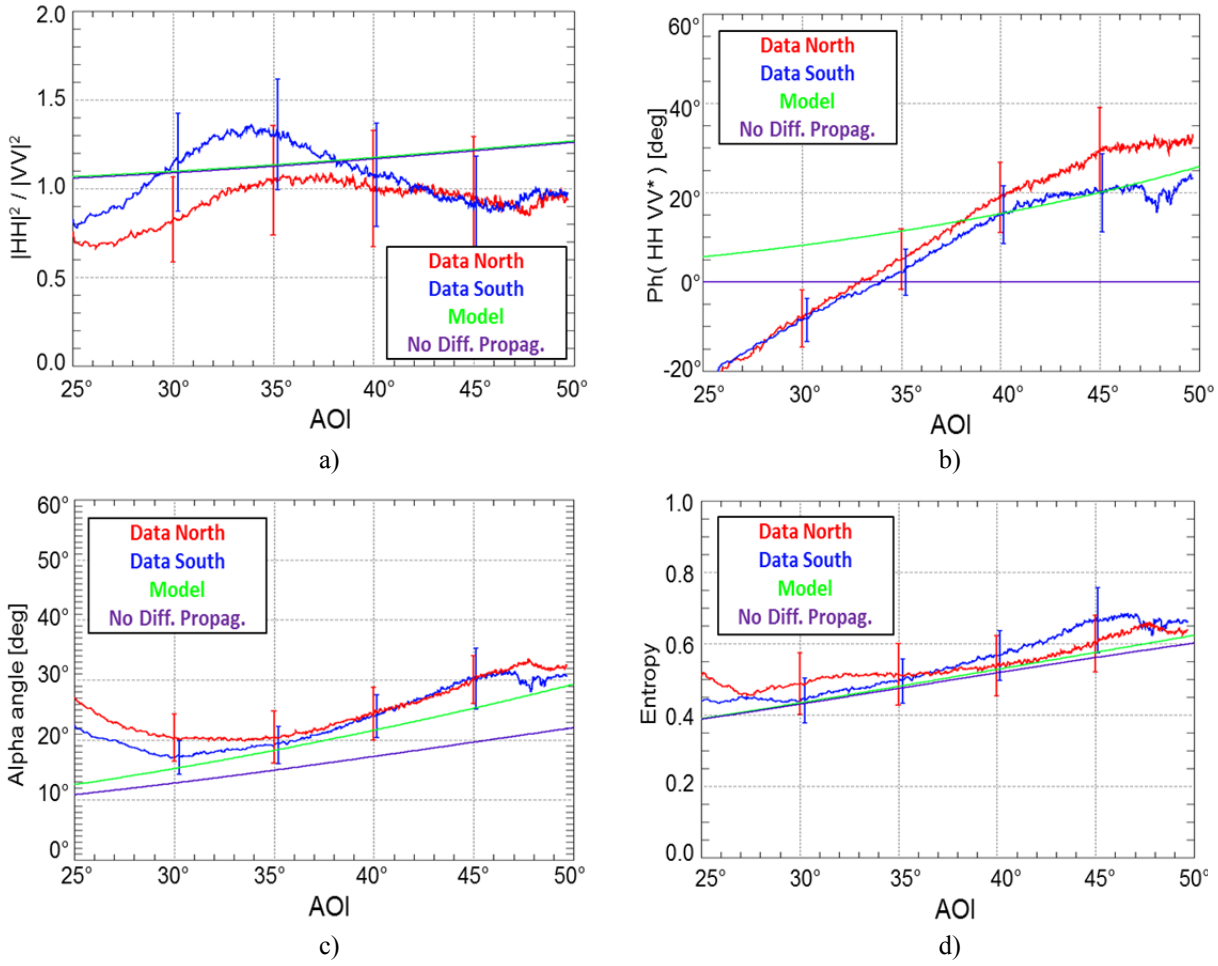

Figure 4: Model-to-data comparison of the selected polarimetric signatures at P-band: co-polarization ratio (a), co-polarization phase difference (b), mean alpha angle (c) and entropy (d). Red and blue lines refer again to observed range profiles for north and south headings, respectively; green lines indicate modeled signatures including differential propagation effects whereas purple lines refer to the case that does not account for this phenomenon.

The model-to-data comparison clearly shows that the introduction of differential propagation effects related to the firn anisotropy is crucial for a correct interpretation of the signatures observed in the data. In particular for the L-band case, the model provides a satisfactory agreement with the data, being able to predict also the observed co-polarization phase difference. Differential propagation has significant impact also on the explanation of entropy and alpha angle values. Finally, the possibility to model the shape of the scatterers (A_p) allows an interpretation of the values and range trend of the co-polarization ratio. At P-band, the deeper penetration depth emphasizes the presence of local buried structures that are not explicitly included in the model. This can be seen as a proof that the developed approach works properly when homogeneous scenarios are considered, as the L-band case.

REFERENCES

1. Rignot, E. (1995). Backscatter Model for the Unusual Radar Properties of the Greenland Ice Sheet. *Journal of Geophysical Research*, 100 (E5), 9389-9400.

2. Sharma, J., Hajnsek, I., Papathanassiou, K.P., and Moreira, A. (2011). Polarimetric Decomposition Over Glacier Ice Using Long-wavelength Airborne PolSAR. *IEEE Trans. Geosci. Remote Sens*, 49 (1), 519-535.

3. Jezek, K.C., Gogineni, P., and Shanableh, M. (1994). Radar Measurements of Melt Zones on the Greenland Ice Sheet. *Geophysical Research Letters*, 21(1), 33-36.

4. Langley, K., Lacroix, P., Hamran, S.E., and Brandt, O. (2009). Sources of Backscatter at 5.3 GHz from a Superimposed Ice and Firn Area Revealed by Multi-

frequency GPR and cores. *Journal of Glaciology*, 55(190), 373-383.

5. Parrella, G., Al-Kahachi, N., Jagdhuber, T., Hajnsek, I., and Papathanassiou, K.P. (2012). Ice Volume Characterization using Long-Wavelength Airborne PolSAR Data. *Proceedings of IEEE IGARSS 2012*, Munich, Germany, 3245-3248.

6. Alley, R.B. (1987). Texture of Polar Firn for Remote Sensing. *Annals of Glaciology*, 9, 1-4.

7. Cloude, S.R., Papathanassiou, K.P., and Boerner W.M. (2000). The Remote Sensing of Oriented Volume Scattering Using Polarimetric Radar Interferometry. *Proceedings of ISAP*, Fukuoka, Japan, pp. 549-552.

8. Sihvola, A. (2000). Mixing Rules with Complex Dielectric Coefficients. *Subsurface Sensing Technologies and Applications*, 1(4), 393-415.

9. Maetzler, C., and Wegmueller, U. (1987). Dielectric Properties of Fresh-water Ice at Microwave Frequencies. *J. Phys. D: Appl. Phys.*, (20), 1623-1630.

10. Ulaby, F.T., Moore, R.K., and Fung, A.K. (1981). Microwave Remote Sensing, Active and Passive, Volume II: Fundamentals and Radiometry, Norwood, MA: Addison-Wesley.

11. Dunse, T., Schuler, T.V., Hagen, J.O., Eiken, T., Brandt, O., and Hogda, K.A. (2009). Recent Fluctuations in the Extent of the Firn Area of Austfonna, Svalbard, Inferred from GPR. *Annals of Glaciology*, 20, 155-162.